

Photon Splitting and Pair Conversion in Strong Magnetic Fields

Matthew G. Baring

Rice University, Department of Physics and Astronomy - MS 108,
P. O. Box 1892, Houston, Texas 77251-1892, USA
baring@rice.edu

Abstract The magnetospheres of neutron stars provide a valuable testing ground for as-yet unverified theoretical predictions of quantum electrodynamics (QED) in strong electromagnetic fields. Exhibiting magnetic field strengths well in excess of a TeraGauss, such compact astrophysical environments permit the action of exotic mechanisms that are forbidden by symmetries in field-free regions. Foremost among these processes are single-photon pair creation, where a photon converts to an electron-positron pair, and magnetic photon splitting, where a single photon divides into two of lesser energy via the coupling to the external field. The pair conversion process is exponentially small in weak fields, and provides the leading order contribution to vacuum polarization. In contrast, photon splitting possesses no energy threshold and can operate in kinematic regimes where the lower order pair conversion is energetically forbidden. This paper outlines some of the key physical aspects of these processes, and highlights their manifestation in neutron star magnetospheres. Anticipated observational signatures include profound absorption turnovers in pulsar spectra at gamma-ray wavelengths. The shapes of these turnovers provide diagnostics on the possible action of pair creation and the geometrical locale of the photon emission region. There is real potential for the first confirmation of strong field QED with the new GLAST mission, to be launched by NASA in 2008. Suppression of pair creation by photon splitting and its implications for pulsars is also discussed.

Keywords : Quantum Electrodynamics, Magnetic Fields, Neutron Stars, Pulsars.

1 Introduction

Quantum Electrodynamics (QED) is one of the most robust theories of physics. It has been extensively and almost exhaustively tested in terrestrial laboratory experiments, as have its constituent, ingredient disciplines, special relativity and quantum mechanics. The thoroughness of its investigation has forged an extreme confidence in the physics community in the viability of its predictions, and its broad applicability in Nature. This has naturally extended to astrophysical settings, where both the more conventional and even the more exotic processes from QED are applied in models of different sources of radiation. Foremost among these are Compton scattering $e\gamma \rightarrow e\gamma$ and two-photon pair creation, $\gamma\gamma \rightarrow e^+e^-$, which have been precisely calculated and tested since the 1930s as processes that are probable in the

cosmos due to their comparatively high cross sections. Because they most generally apply to relativistic environs where X-rays and gamma-rays abound, they are ubiquitous in models of compact, non-magnetic astrophysical systems, particularly those involving black holes, both galactic (typically with masses M of a few solar masses M_\odot), and extragalactic and supermassive (with $M \sim 10^6 - 10^9 M_\odot$).

Neutron stars, compact remnants of aged stars more massive than the sun that have undergone a supernova event, provide a very different environment for physical processes. Supported only by neutron degeneracy pressure against the incredibly compressing pull of gravity, they stably exist with radii R_{NS} of the order of 10 km. During the supernova core implosion, it is believed that charge currents in their outer layers persist and strengthen so that their magnetic fields intensify, perhaps exceeding magnetic flux conservation. They can then possess fields in the range of $10^{10} - 10^{15}$ Gauss (i.e., $10^6 - 10^{11}$ Tesla; see, e.g. [1, 2]) that are far beyond the realm of terrestrial experiments. The prime observational manifestations of neutron stars are pulsars, rapidly pulsating radio sources that were discovered in 1967 [3]. Now seen in other wavebands such as the optical, X-rays and gamma-rays, their interpretation as rapidly rotating neutron stars [4] that slowly *spin down* to longer pulse periods has provided powerful evidence for the existence of strong \mathbf{B} fields. This evidence is derived from a rotating, tilted dipole model for the field structure [5, 6], the rotational/electromagnetic torque on which leads to inferences of surface fields in the range $B \sim 10^9 - 10^{15}$ Gauss. Such a dipole picture is the simplest choice for the field geometry, being the leading order moment for any magnetic field configuration. The rotation and magnetic axes are generally not aligned, just as in the cases of the sun and the Earth, and so the time-varying \mathbf{B} fields induce electric fields \mathbf{E} of substantial magnitude above the stellar surface. These \mathbf{E} fields are quenched [5, 6] on relatively small lengthscales by charges that are prolifically created via the magnetic pair production process that is detailed in this paper. Furthermore, note that additional support for the existence of such intense \mathbf{B} fields comes from spectroscopic observations of putative cyclotron emission or absorption lines in the 20–150 keV band of accreting X-ray binary pulsars [7]. A discussion of these pertinent astrophysical elements can be found in [2].

These strong field environs provide an opportunity for more exotic and less familiar predictions of QED to come to the fore. The \mathbf{B} field profoundly changes the physical nature of quantum interactions, yielding a strong bias towards momentum exchange along the field. It quantizes the electron states in a direction perpendicular to the field so that momentum in that direction is no longer conserved; a product of the lack of translational invariance of the states orthogonal to \mathbf{B} . Accordingly, $B = 0$ symmetries are broken, and interactions that are forbidden in field-free environs become possible, and even probable in neutron star magnetospheres. The most likely among these are magnetic pair creation $\gamma \rightarrow e^+e^-$ and photon splitting $\gamma \rightarrow \gamma\gamma$. These are more recent predictions of QED, dating from the 1950s and 1960s, partly due to their inherent mathematical complexity (spawned by quanti-

zation in a cylindrical geometry), and partly due to the contemporaneous rising interest in their applicability to cosmic systems, e.g. neutron stars. The fact that these, as yet, untested predictions of QED are widely invoked in pulsar contexts is a true testament to physicists' confidence in the theory of relativistic quantum mechanics. These two processes form the focus of this paper, though it is noted that strong-field quantum effects also have profound influences on Compton scattering [8, 9], classical synchrotron radiation [10, 11], and other radiation processes.

2 Magnetic Pair Creation

One-photon pair production $\gamma \rightarrow e^+e^-$ in strong magnetic fields is a first-order QED process with one vertex that is quite familiar to pulsar theorists, having been invoked in polar cap models to explain the photon emission of both radio pulsars (e.g. [5, 6]) and the handful of known gamma-ray pulsars (e.g. [12]). It is forbidden in field-free regions due to the imposition of four-momentum conservation, but takes place in an external magnetic field, which can absorb momentum perpendicular to \mathbf{B} (momentum along the field is still conserved, as is the energy). The first analytic computations of its rate R^{pp} [13, 14] (hereafter the superscript **pp** denotes pair production) indicated a rapid rise with increasing photon energy ε_γ and magnetic field strength, becoming significant for γ -rays above the pair threshold, $\omega \equiv \varepsilon_\gamma/(m_e c^2) = 2/\sin \theta_{\text{kB}}$, and for fields approaching the quantum critical field

$$B_{\text{cr}} = \frac{m_e^2 c^3}{e \hbar} \approx 4.413 \times 10^{13} \text{ Gauss} \quad . \quad (1)$$

Here θ_{kB} is the angle the photon momentum vector \mathbf{k} makes with the magnetic field \mathbf{B} . B_{cr} represents the field at which the cyclotron energy equals $m_e c^2$, and defines the field scale at which the impact of the external \mathbf{B} field on quantum processes becomes significant. It is appropriate to identify now the dimensionless scaling conventions to be adopted throughout this paper that are of common usage. All photon energies, ω , will be scaled in terms of the electron rest mass energy $m_e c^2$, and all field strengths will hereafter be expressed in terms of B_{cr} , i.e. $B = 1$ denotes a field of 4.413×10^{13} Gauss. We note in passing that pair creation $\gamma \rightarrow e^+e^-$ in the induced electric fields is also possible in rotating pulsar magnetospheres, however this is reduced by the order of $v_{\text{rot}}/c \ll 1$ near the neutron star surface due to corotation speeds $v_{\text{rot}} = 2\pi R_{\text{NS}}/P$ usually being relatively small (R_{NS} is the neutron star radius and P is the pulsar period).

The magnetic pair creation rate is resonant at the thresholds for each combination of produced pair states, due to the available momentum parallel to the field approaching zero in the frame where $\theta_{\text{kB}} = \pi/2$. A large number of integrable (over photon energies) resonances result, producing a characteristic sawtooth structure [15, 16] that is displayed in Figure 1 below. In astrophysical contexts, a range of field strengths and initial photon energies ω are always sampled, and the resulting

convolution smears out the sawtooth appearance into a continuum. Fully general expositions of the $\gamma \rightarrow e^+e^-$ rate in uniform \mathbf{B} fields can be found in [10, 15]. Here we highlight the spectral structure near absolute pair threshold $\omega = 2/\sin\theta_{\text{kB}}$, a case most germane to pulsar applications since generally photons are produced in beams almost along the local field lines in the dipole geometry, so that pair creation threshold is crossed from below during magnetospheric propagation of photons. This implies that calculations in the domain $\omega \gtrsim 2/\sin\theta_{\text{kB}}$ are typically of greater practical relevance, especially for near-critical or supercritical fields $B \gtrsim 0.1$ [17]. The pertinent rates, exhibited in [17], can be written as follows. Let (j, k) denotes the Landau level quantum numbers of the produced pairs, which have energies $\sqrt{1 + p_{jk}^2 + 2jB}$ and $\sqrt{1 + p_{jk}^2 + 2kB}$. The parallel momenta p_{jk} of the pairs in the frame of reference for photons moving perpendicular to the field are given by

$$|p_{jk}| = \left[\frac{\omega^2}{4} \sin^2 \theta_{\text{kB}} - 1 - (j+k)B + \left(\frac{(j-k)B}{\omega \sin \theta_{\text{kB}}} \right)^2 \right]^{1/2}, \quad (2)$$

with the solution of $p_{jk} = 0$ defining the host of resonant energies ω . Throughout, electron energies are scaled by $m_e c^2$ and their momenta are in terms of $m_e c$.

Near threshold, only a few pair states are kinematically accessible. The rates are dependent on the polarization of the incoming photon. Following common practice, here we adopt the convention that photon linear polarizations are such that \parallel refers to the state with the photon's *electric* field vector parallel to the plane containing the magnetic field and the photon's momentum vector, while \perp denotes when the photon's electric field vector is normal to this plane. Let $\lambda = \hbar/m_e c$ be the Compton wavelength of the electron over 2π , and $\alpha_f = e^2/\hbar c$ be the fine structure constant. The exact, polarization-dependent, pair production rate [15], including only the $(j=0, k=0)$ pair state for \parallel polarization is:

$$R_{\parallel}^{\text{pp}} = \frac{\alpha_f c}{\lambda} \frac{\sin \theta_{\text{kB}}}{\xi |p_{00}|} \exp(-\xi) \quad , \quad \omega \geq \frac{2}{\sin \theta_{\text{kB}}} \quad , \quad (3)$$

for $\xi = \omega^2 \sin^2 \theta_{\text{kB}}/[2B]$, while the sum of the $(j=0, k=1)$ and $(j=1, k=0)$ states contributes just above threshold for the \perp polarization:

$$R_{\perp}^{\text{pp}} = \frac{\alpha_f c}{\lambda} \frac{\sin \theta_{\text{kB}}}{\xi |p_{01}|} (E_0 E_1 + 1 + p_{01}^2) \exp(-\xi) \quad , \quad \omega \geq \frac{1 + \sqrt{1 + 2B}}{\sin \theta_{\text{kB}}} \quad . \quad (4)$$

The pertinent dimensionless energies of the produced pairs are

$$E_0 = \sqrt{1 + p_{01}^2} \quad , \quad E_1 = \sqrt{1 + p_{01}^2 + 2B} \quad . \quad (5)$$

Observe that the absolute threshold for \perp photons is higher than that for \parallel photons, an effect that finds its origin in the spin-dependence of energies in the final pair states. Indeed, the rate for the \perp state is always lower than that for the \parallel state. This property for the leading order photon absorption process, when connected via

the optical theorem to the consideration of dispersion in the magnetized vacuum, clearly indicates that such a vacuum is birefringent.

For photon energies well above threshold, the number of accessible pair states becomes very large, much larger than just the few states considered above (see Figure 1 for an illustration of the sawtooth resonant structure of the rates). Then the resonances at $p_{jk} = 0$ tend to blend into one another, an effect that is enhanced in pulsar magnetospheres by sampling significant ranges of photon energies, angles and field strengths that smear out the cusp-like structure in forming an average reaction rate. In this regime, the dependence on ω can be averaged over ranges larger than the typical separation of the resonances, and one can use more convenient asymptotic expressions for the polarization-dependent pair creation rates [14, 18, 19]:

$$R_{\parallel}^{\text{pp}} \approx 2R_{\perp}^{\text{pp}} \approx \frac{1}{2} \sqrt{\frac{3}{2}} \frac{\alpha_{\text{f}} c}{\lambda} B \sin \theta_{\text{KB}} \exp\left\{-\frac{8}{3\chi}\right\}, \quad \chi \equiv \omega B \sin \theta_{\text{KB}} \ll 1, \quad (6)$$

where χ is the critical asymptotic expansion parameter. These results essentially derive from Schwinger-type mathematical formulations, as do alternative results (e.g. [18, 19]) for the $\chi \gg 1$ regime that are generally of less practical interest. The differences between the asymptotic result in Eq. (6) and the exact rates become profound near threshold [15], and the asymptotic analyses can be improved considerably by treating mildly-relativistic regimes for the produced pairs [11, 16].

As mentioned above, in polar cap pulsar models [5, 6, 12], high energy radiation is usually emitted at very small angles to the magnetic field, well below pair threshold [17]. The γ -ray photons will convert into pairs only after traveling a distance s that is a fraction of the field line radius of curvature ρ_c (which exceeds the neutron star radius R_{NS}), so that $\sin \theta_{\text{KB}} \sim s/\rho_c$. From Eq. (6), the pair production rate will be vanishingly small until the argument of the exponential approaches unity, i.e., when $\omega B \sin \theta_{\text{KB}} \gtrsim 0.2$. Consequently, pair production will occur well above threshold when $B \ll 0.1$ and the asymptotic expression will be valid; from Figure 1 one can deduce that the attenuation length will then be much less than R_{NS} . In contrast, when $B \gtrsim 0.1$, pair creation will occur at or near threshold, and Eqs. (3) and (4) become more appropriate. In this domain, an additional subtlety arises, since another mode of pair creation exists, namely the formation of pairs in a bound state, i.e. positronium. This has been proposed as an effective competitor to the production of free pairs [20, 21, 22] because the binding energy lowers the threshold slightly ($\ll 1\%$) below the value for production of free pairs. The relevance of positronium formation to pulsars is potentially great if the bound state is stable for considerable times. Positronium is subject to destruction by three main mechanisms: free decay, electric field ionization, and photo-ionization. As discussed in [17], due to conflicting calculations, it is presently unclear whether or not positronium is stable to free decay and photo-ionization; assessment of this issue motivates future work.

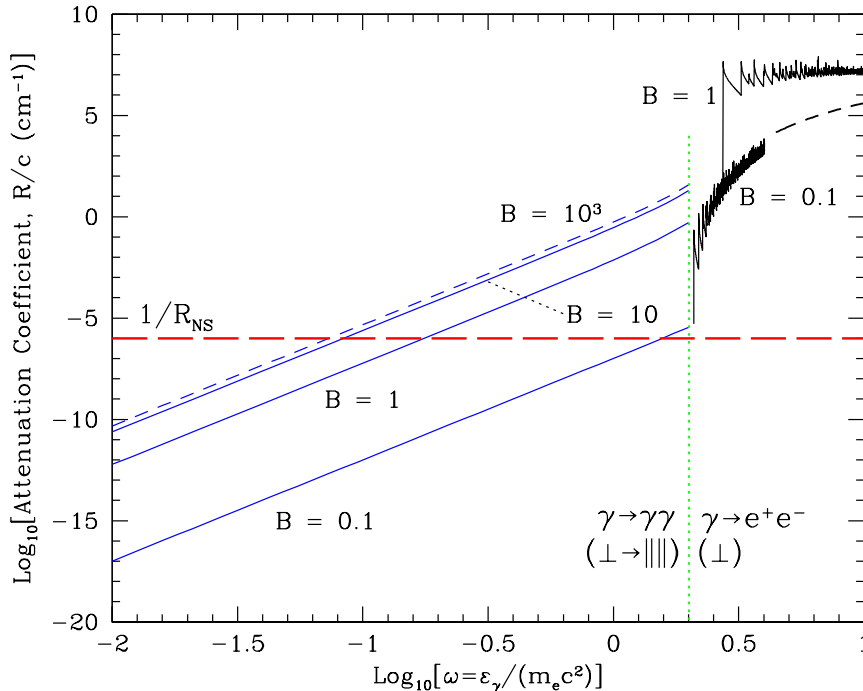


Fig. 1: Attenuation coefficients or inverse attenuation lengths (i.e., rates R_{\perp}^{pp} and $R_{\perp \rightarrow ||||}^{\text{sp}}$ divided by c), for pair creation (above the threshold $\omega = 2$) and photon splitting for the polarization mode $\perp \rightarrow ||||$ (only for $\omega < 2$), as functions of the incident photon energy ω , for field strengths B , as labelled. Photons are assumed to propagate orthogonally to the field lines ($\theta_{\text{KB}} = 90^\circ$). The pair creation rates are computed using [15, 23], and only for \perp photons; at $\omega > 4$ the dashed $B = 0.1$ curve is the asymptotic form in Eq. (6). Also, the dashed splitting curve labelled $B = 10^3$ represents the asymptotic high-field “saturation” result. The horizontal heavy dashed line labelled $1/R_{\text{NS}}$ marks the approximate minimum effective attenuation coefficient for which these processes become prolific in pulsar magnetospheres.

3 Magnetic Photon Splitting

The most important competitor to pair creation $\gamma \rightarrow e^+e^-$ at high magnetic field strengths as a mechanism for attenuating photons in pulsar magnetospheres is magnetic photon splitting $\gamma \rightarrow \gamma\gamma$. The relevance of this process to neutron star environments has been emphasized in various papers [24, 25, 11]. Splitting is a third-order QED process with a triangular Feynman diagram, and therefore is weaker than magnetic pair creation by the order of α_f^2 , yet without the constraint of a threshold energy, an important distinction. Though splitting is permitted by energy and momentum conservation, when $B = 0$ it is forbidden by a charge conjugation symmetry of QED known as Furry’s theorem (e.g. [26]), which states that ring diagrams that have an odd number of vertices with only external photon lines generate

interaction matrix elements that are identically zero. The presence of an external field breaks this symmetry. The splitting of photons is therefore a purely quantum effect, and has appreciable reaction rates only when $B \gtrsim 1$.

Magnetic splitting $\gamma \rightarrow \gamma\gamma$ is a relatively recent prediction of QED. A decade of controversy followed the earliest calculations in the 1960s before the first correct evaluations of its rate [24, 27, 28] were performed, via an effective Lagrangian technique. These works focused on asymptotic forms in the limit of photon energies well below pair creation threshold, which varied as B^6 when $B \ll 1$. Their rate determinations neglected dispersion in the birefringent, magnetized vacuum, so that all photon momenta were assumed collinear. The early controversy was fueled by the inherent difficulties in calculating the rates of this third order process by standard QED techniques, an issue that re-emerged in the 1990s (see [23] for a discussion). For weak-dispersion regimes, fully general rates in Schwinger-type formalisms were derived by various groups [24, 29, 30, 31]. Even more general S-matrix, Landau representation calculations that include information on the pair resonances are derived by [32] and [33, 34] (note that issues concerning the erroneous numerics in [32] are addressed in [23]). These resonances are a significant factor in determining the splitting rate near and above pair threshold, since then the intermediate pair states go “on-shell” and the splitting process effectively becomes first-order in α_f , tantamount to a pair conversion followed by cyclotron decays.

It is practical to restrict considerations of splitting to regimes of weak dispersion, where manageable expressions for its rates are obtainable. These are still complicated triple integrations in Schwinger formalisms [24, 29, 30, 31] or triple summations in S-matrix calculations [34]. Further specialization to either low magnetic fields ($B \ll B_{\text{cr}}$) or low photon energies ($\omega \ll 2$) therefore proves expedient, and palatable results for splitting rates were first obtained in such regimes. A compact presentation of these rates (i.e. for $\omega \ll 2$) for the three polarization modes of splitting permitted by CP (charge-parity) invariance in QED, namely $\perp \rightarrow \parallel\parallel$, $\perp \rightarrow \perp\perp$ and $\parallel \rightarrow \perp\parallel$, is

$$\begin{aligned} R_{\perp \rightarrow \parallel\parallel}^{\text{sp}}(\omega) &= \frac{\alpha_f^3}{60\pi^2} \frac{c}{\lambda} \omega^5 B^6 \sin^6 \theta_{\text{KB}} \mathcal{M}_1^2 = \frac{1}{2} R_{\parallel \rightarrow \perp\parallel}^{\text{sp}} \\ R_{\perp \rightarrow \perp\perp}^{\text{sp}} &= \frac{\alpha_f^3}{60\pi^2} \frac{c}{\lambda} \omega^5 B^6 \sin^6 \theta_{\text{KB}} \mathcal{M}_2^2 \end{aligned} \quad (7)$$

using the superscript notation **sp** to signify photon splitting. Here the “scattering amplitudes,” which have been computed numerically in [23, 24], are given by

$$\begin{aligned} \mathcal{M}_1 &= \frac{1}{B^4} \int_0^\infty \frac{ds}{s} e^{-s/B} \left\{ \left(-\frac{3}{4s} + \frac{s}{6} \right) \frac{\cosh s}{\sinh s} + \frac{3 + 2s^2}{12 \sinh^2 s} + \frac{s \cosh s}{2 \sinh^3 s} \right\}, \\ \mathcal{M}_2 &= \frac{1}{B^4} \int_0^\infty \frac{ds}{s} e^{-s/B} \left\{ \frac{3}{4s} \frac{\cosh s}{\sinh s} + \frac{3 - 4s^2}{4 \sinh^2 s} - \frac{3s^2}{2 \sinh^4 s} \right\}. \end{aligned} \quad (8)$$

Evaluations of these forms in terms of special functions were obtained in [34]:

$$\begin{aligned}
\mathcal{M}_1 &= \frac{1}{B^3} \left\{ \frac{4}{B} \log_e \Gamma_1\left(\frac{1}{2B}\right) - \frac{1}{2B^2} \log_e \Gamma\left(\frac{1}{2B}\right) - \left(\frac{1}{3B} + \frac{1}{4B^3}\right) \psi\left(\frac{1}{2B}\right) \right. \\
&\quad \left. - \frac{1}{12B^2} \psi'\left(\frac{1}{2B}\right) - \frac{1}{6} - \frac{24L_1 - 1}{6B} - \frac{1}{4B^2} \left(\log_e \frac{4B^3}{\pi} + 1 \right) \right\} \\
\mathcal{M}_2 &= \frac{1}{B^3} \left\{ -\frac{3}{2B^2} \log_e \Gamma\left(\frac{1}{2B}\right) + \frac{3}{4B^3} \psi\left(\frac{1}{2B}\right) \right. \\
&\quad \left. + \frac{1}{8B^4} \psi'\left(\frac{1}{2B}\right) + \frac{1}{3B} + \frac{1}{2B^2} - \frac{1}{B^3} + \frac{3}{4B^2} \log_e 4\pi B \right\},
\end{aligned} \tag{9}$$

where $\Gamma(x)$ is the Gamma function, $\psi(x) = d \log_e \Gamma(x)/dx$ is the digamma function, $L_1 \approx 0.24875$ is a constant resulting from the sum of the logarithmic series that expresses the remainder for Stirling's approximation for the Γ function, and

$$\log_e \Gamma_1(x) = \int_0^x dt \log_e \Gamma(t) + \frac{1}{2} x(x-1) - \frac{x}{2} \log_e 2\pi. \tag{10}$$

At low fields, $\mathcal{M}_1 \approx 26/315$ and $\mathcal{M}_2 \approx 48/315$ are independent of B , but at high fields possess $\mathcal{M}_1 \approx 1/(6B^3)$ and $\mathcal{M}_2 \approx 1/(3B^4)$ dependences. Hence, the rate for $\perp \rightarrow \parallel\parallel\parallel$ asymptotically approaches a constant as $B \rightarrow \infty$, a result that is exhibited in Figure 1. These rates are of broad applicability to pulsar modeling. Deviations from this low energy limit near pair creation threshold are detailed by [23, 30, 34]; they are somewhat apparent in Figure 1, for which the numerics were obtained from the full Schwinger-type results of [23]. Note that the B^6 dependence of the rates when $B \ll 1$ permits the use of so-called hexagon Feynman diagrams when treating the field as a small perturbation at three vertices, a technique employed in early computations of this process. This approximation cannot be used for higher B where the field's influence on the electron propagators must be incorporated self-consistently, and results in greater complexity as appears in Eq. (8).

As mentioned in Section 2, the different pair creation attenuation rates for the two linear polarization states automatically generate polarization-dependent refractive indices ($n_\perp \neq n_\parallel$) and light speeds, i.e. birefringence. This birefringence of the magnetized vacuum also implies an alteration of the kinematics of strong field QED processes [24], admitting the possibility of non-collinear photon splitting. Hence, while the splitting modes $\perp \rightarrow \perp\parallel$, $\parallel \rightarrow \perp\perp$ and $\parallel \rightarrow \parallel\parallel$ are forbidden by CP invariance in the limit of zero dispersion, dispersive effects guarantee a small but non-zero probability for the $\perp \rightarrow \perp\parallel$ channel. Extensive discussions of linear dispersion in a magnetized vacuum [24, 35] demonstrate that in the limit of *weak linear vacuum* dispersion (roughly delineated by $B \sin \theta_{\text{KB}} \lesssim B_{\text{cr}}$), where the refractive indices for the polarization states are very close to unity, energy and momentum could be simultaneously conserved only for the splitting mode $\perp \rightarrow \parallel\parallel$ (of the modes permitted by CP invariance) below pair production threshold.

This result, known as Adler’s [24] kinematic selection rules for photon splitting, is contingent upon the inequality $R_{\perp}^{pp} < R_{\parallel}^{pp}$, assuming that pair creation $\gamma \rightarrow e^+e^-$ provides the dominant contribution to the vacuum dispersion, generally true for $B \ll 1$ regimes of low plasma density.¹ Therefore, it is probable that only the one mode ($\perp \rightarrow \parallel \parallel$) of splitting operates in normal pulsars. However, this constraint may not hold in supercritical fields where stronger vacuum dispersion arises and other contributions may come into play. For example, the generalized vacuum polarizability tensor may yield significant corrections from quadratic (i.e. those that connect to photon splitting) and higher order contributions. Recent analysis [37] of vacuum dispersion induced only by pair attenuation has indicated that while the selection rules are generally upheld as ω increases towards pair threshold, they have to be modified in certain phase spaces above pair threshold. In such regimes, splitting cannot be discounted relative to $\gamma \rightarrow e^+e^-$ as a higher order process, since its rates sample pair resonances when the electron propagators go “on-shell,” and the splitting rate may approach that of a first-order process. Such calculations of rates for $\gamma \rightarrow \gamma\gamma$ at $\omega > 2/\sin\theta_{\text{kB}}$ have not yet been performed at any length, though the formulations of [32, 34] can be readily applied to this problem.

4 Anticipated Astrophysical Signatures

Having encapsulated the essentials of the physics of these two exotic predictions of high-field quantum electrodynamics, the focus now turns to how signatures of these processes might realistically manifest themselves in pulsars. It is quite possible that a vindication in astrophysical contexts for the theoretical expectations may predate the eventual first observation of either process in terrestrial laboratories.

4.1 Pair Creation

Since the magnetic pair creation rate is generally a strongly increasing function of photon energy, its major signature is an attenuation turnover in pulsar radiation spectra. The resulting maximum energy of emission is controlled by attenuation during photon propagation through the pulsar magnetosphere. Such attenuation provides a characteristic super-exponential turnover [38] (see below) that contrasts that expected in outer gap models (e.g. see [39, 44] for a comparison), scenarios where the gamma-rays are generated in a pulsar’s outer magnetosphere and the quantum effects discussed here are negligible. Pair creation effectively occurs at the threshold $\omega \sin\theta_{\text{kB}} = 2$ for high fields, i.e. $B \gtrsim 1$, and above threshold at $\omega \sin\theta_{\text{kB}} \sim 0.2/B$ for lower fields [15]. Hence, the mean free path for photon attenuation in *curved* fields is $\lambda_{\text{pp}} \sim \rho_c/\omega \max\{2, 0.2/B\}$, i.e. usually when $\omega \sin\theta_{\text{kB}}$ crosses above threshold during propagation. This assertion derives from the fact that

¹ Note that in the dense gases encountered deep in neutron star atmospheres, dispersion becomes dominated by plasma contributions [36], for which the selection rules of Adler are not applicable.

photons are generally emitted almost parallel to the local \mathbf{B} due to the relativistic beaming associated with electrons/pairs streaming along the field lines. The radius of field curvature at altitude $R_0 \geq R_{\text{NS}}$ is $\rho_c = [P R_0 c / 2\pi]^{1/2}$ for a pulsar period P . This introduces a dependence of the energy when pair threshold is crossed of $\omega \propto 1/\theta_{\text{KB}} \propto \rho_c \propto \sqrt{P R_0}$. In a dipole field geometry, the local magnetic field scales as $B \propto R_0^{-3}$, thereby generating the scaling $\omega \propto 1/B \propto R_0^3$ for the energy of photons that access pair threshold. Accordingly, the approximate dependence of pair creation cutoff energies ε_{MAX} on the surface polar field strength B_0 , altitude R_0 and pulsar period P (in seconds) can be summarized in the approximate empirical relation (e.g. [40] and references therein)

$$\varepsilon_{\text{MAX}} \approx 0.4\sqrt{P} \left(\frac{R_0}{R_{\text{NS}}} \right)^{1/2} \max \left\{ 1, \frac{0.1}{B_0} \left(\frac{R_0}{R_{\text{NS}}} \right)^3 \right\} \text{ GeV} . \quad (11)$$

Accurate numerical determinations of the turnover maximum energy from the codes developed in [41, 17], are plotted in Figure 2; these include the effects of general relativity on spacetime curvature, field enhancement and photon energy in “slowly-rotating” systems with $P \gg 2\pi R_{\text{NS}}/c$. At fields $B_0 \gtrsim 0.7$ photon splitting acts to further reduce ε_{MAX} , as discussed in [17], though not shown in the Figure here.

Figure 2 and Eq. (11) clearly indicate a strong anti-correlation between the maximum energy and the surface magnetic field. Coupled with observed maximum energies in pulsars detected by the Compton Gamma-Ray Observatory (CGRO), this behavior seems to be augmented by an apparent decline of emission altitude with B_0 . Such a trend, which is not anticipated in outer gap models, is a distinctive characteristic that can be probed by NASA’s upcoming Gamma-Ray Large Area Space Telescope (GLAST, to be launched in mid-2008). This core NASA astrophysics mission is expected to add at least 50-100 pulsars to the extant database, possibly many more, perhaps around half of which will offer clean ε_{MAX} determinations to refine Figure 2 further. The maximum energy is generally in the 1–10 GeV band for normal young pulsars, but can be much lower [41, 17] for highly magnetized ones, and also much higher for millisecond pulsars, so that signals in the 30–100 GeV band are possible [42, 43] for polar cap models via synchrotron/curvature cascades if the field is low enough.

Such a statistical correlation for a population of pulsars is not the only signature of the operation of $\gamma \rightarrow e^+e^-$. Normally, maximum energy turnovers resulting from a moderately energy-dependent attenuation of photons in astronomical sources assume an exponential form $dn_\gamma/d\varepsilon_\gamma \propto \exp\{-\varepsilon_\gamma/\varepsilon_{\text{cutoff}}\}$. In this particular instance, the attenuation process is exponentially-sensitive [as evinced in Eq. (6)] to the incoming photon energy for subcritical field strengths; a similarly rapid onset should be experienced when $B \gtrsim 1$. The upshot is that magnetic pair creation should impose a *super-exponential* cutoff in pulsar gamma-ray spectra of the approximate form $dn_\gamma/d\varepsilon_\gamma \propto \exp\{-\alpha \exp[-\varepsilon_{\text{MAX}}/\varepsilon_\gamma]\}$ for some constant α . The severity of the cutoff will depend on the range of altitudes and magnetic latitudes sampled in the

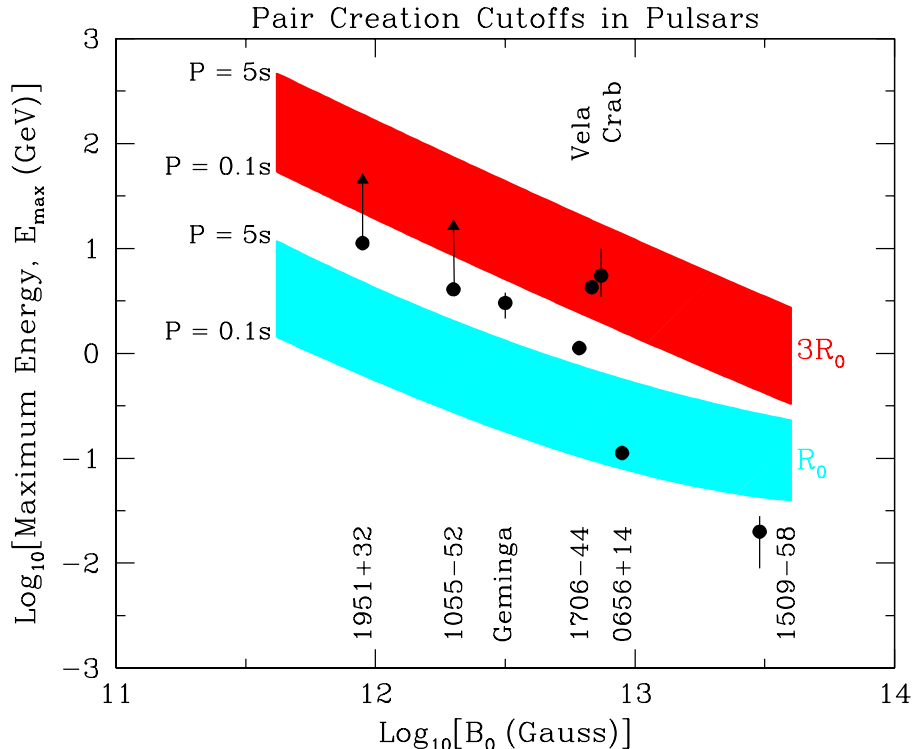


Fig. 2: Maximum pulsar emission energies (adapted from [40]) imposed by pair creation attenuation at two different altitudes, R_0 (dashed curves) and $3R_0$ (solid curves), described empirically via Eq. (11). For each altitude, a range of pulse periods (polar cap sizes) 0.1 – 5 sec is represented, as indicated. These energies are determined by the comprehensive photon propagation/attenuation code described in [17], which includes curved spacetime effects. Observed/inferred cutoff energies (or ranges) for 8 gamma-ray pulsars of different B_0 are indicated, from which a trend of declining altitude of emission with increasing surface polar field B_0 is suggested.

emission region, but the net result is typically [12, 38] a sharp turnover that is distinguishable from those generated by other attenuation processes. It is anticipated that GLAST will clearly be able to discern such super-exponential cutoffs, if they are present, in a number of pulsars, and accordingly offer discrimination between the viability of polar cap and outer gap models for high energy pulsar emission [44].

The presence of strong fields virtually guarantees a strong polarization signal in polar cap models, and when these couple with spectral structure and temporal information, particularly powerful observational diagnostics are possible. Due to the polarization-dependence of the pair production rates, this may provide a potentially fruitful tool, particularly for highly-magnetized pulsars with $B \gtrsim 10^{13}$ Gauss, since the attenuation cutoffs fall in the 1-10 MeV band. Hard gamma-ray pair production tracking experiments like GLAST are generally not afforded the opportunity to act as polarimeters, being limited by multiple scattering in tracking chambers above

300 MeV. Medium energy gamma-ray experiments, on the other hand, are ideally suited to polarization studies, essentially via their sampling of Compton scattering kinematics. Gamma-ray polarimetry is no longer a distant dream [45]. Europe’s current INTEGRAL mission, and NASA’s solar RHESSI telescope have some ability to detect polarization in bright sources such as gamma-ray bursts [46, 47] and X-class solar flares. Moreover, polarimetric capability in the hard X-ray and soft gamma-ray bands is a high priority for next-generation tracking Compton detectors such as the Advanced Compton Telescope experimental initiative [48].

As an interesting aside pertaining to a completely different astrophysical context, it is worth noting that opacities for pair creation are currently included in simulation codes for the propagation of ultra-high energy cosmic rays and air shower initiation in the Earth’s upper atmosphere and magnetosphere. This presumes a possibility that these energetic particles could be photons, something that is currently not a popular perception, but has not yet conclusively been excluded. For completeness, the shower simulations for ground-based detector arrays (e.g. [49, 50]) such as Fly’s Eye/HIRES, AGASA and Auger include $\gamma \rightarrow e^+e^-$ rates when treating photon primaries, which for terrestrial fields of $B \sim 1 - 10$ Gauss sample the asymptotic regime in Eq. (6). Any photons in the $\varepsilon_\gamma \sim 10^{20}$ eV domain can effectively convert into pairs off the geomagnetic field above the ionosphere and thereby instigate a so-called “pre-shower” that is subsequently reprocessed in a complicated hadronic cascade in the atmosphere below. Such a convolution of interactions precludes definitive determination of the action of $\gamma \rightarrow e^+e^-$ even if a photon primary origin were eventually concluded. Yet a remarkable aspect of this field is that the participating physicists attribute much greater certainty to the strong-field QED physics than to extrapolations of $B = 0$ photonuclear cross sections to such extreme energies.

4.2 Photon Splitting

It is clear from the rates displayed in Figure 1 that the necessary requirement for photon splitting to operate in pulsar magnetospheres is that $B \gtrsim 1$. This turns the focus to a small subset of known neutron stars/pulsars that possess ultrastrong fields, termed *magnetars*. Observations at X-ray energies have yielded detections of both long periods and high period derivatives in two types of such sources, anomalous X-ray pulsars (AXPs) and soft γ -ray repeaters (SGRs), which suggest dipole spin-down fields in the range $10^{14} - 10^{15}$ Gauss. The AXPs are a group of seven or eight pulsating X-ray sources with periods in the range 6–12 seconds, and are continuously spinning down [51]. The SGRs are a type of γ -ray transient source that undergoes repeated bursts, some of them enormous (e.g. [52]); four are definitively known to exist. With the possible exception of the unconfirmed reports [53] of a low frequency pulsed detection of a counterpart (PSR J1907+0919 at 111 MHz) to the soft gamma repeater SGR 1900+14, none of these sources has detectable pulsed radio emission. It is notable, however, that an unusual related source, the transient AXP XTE J1810-197, has exhibited transient and peculiar pulsed radio emission [54].

A central principal of the radio pulsar paradigm is that the emission is coupled to a prolific presence of pairs [5, 6]. As pulsars age, their periods lengthen, due to the action of magnetic dipole radiation torques. Concomitantly, the geometrical confines for their acceleration and emission locales on open field lines become more constricted, roughly as the polar cap opening angle $\Theta_{\text{cap}} \approx [2\pi R_{\text{NS}}/(Pc)]^{1/2}$ shrinks. This establishes a beaming of radiation generated by accelerated pairs, and the collimation angles θ_{KB} for potentially pair producing photons drop. Eventually, the traversal distance in the magnetosphere required to cross pair threshold exceeds the scale for magnetic field decline (i.e. $\sim R_{\text{NS}}$). Pair creation then shuts off, and presumably so does the radio emission, i.e. radio pulsars “die.” This has led to the concept of a pulsar *death line* at long periods, something that is illustrated in Figure 3, which is the P - \dot{P} diagram, the conventional depiction of pulsar phase space. The location of this boundary depends on observables P and the period time derivative \dot{P} , through the relation for the polar field B_0 that is inferred for magnetic dipole torques seeding rotational deceleration (e.g. [17]):

$$B_0 = 6.4 \times 10^{19} [P \dot{P}]^{1/2} \text{ Gauss} \quad . \quad (12)$$

Dotted diagonal lines in Figure 3 denote contours of constant field strength. The locations of over 1500 observed radio pulsars are marked in this Figure. Three of the 8 known gamma-ray pulsars, namely the Crab, Vela and PSR 1509-58 are also highlighted (see lower inset), together with the positions of five radio-quiet anomalous X-ray pulsars (filled green triangles) and SGRs 0526-66, 1806-20 and 1900+14 (filled red squares) in the upper right, constituting the sub-class of magnetars.

An alternative mechanism for suppression of radio emission, specifically in high field pulsars and magnetars, was proposed by [55, 17]. For local fields $B \gtrsim 1$, photon splitting can be an effective competitor to pair creation. This arises principally because the pair threshold is crossed only after emitted photons are transported through the magnetosphere to acquire significant angles with respect to field lines. During this time, when $B \gg 1$, photon splitting can have time to act, and its probability of attenuating the photons and pushing them further below pair threshold by energy degradation is sensitive to the local field strength B and the polar cap geometry, i.e. Θ_{cap} . Consequently, the competition between splittings $\perp \rightarrow \parallel\parallel$ and pair conversions $\perp \rightarrow e^+e^-$ is defined by the principal pulsar observables P and \dot{P} . Detailed discussions and computations of this competition are presented in [55, 17]. They include all the features of QED discussed above, and the general relativistic distortions of the magnetosphere and the photon trajectories in a Schwarzschild geometry. The principal result is an identification of the approximate P and \dot{P} pulsar phase space when it is anticipated that photon splitting will dominate pair creation for \perp photons. This is depicted in Figure 3. Since pair suppression is putatively identified with a lack of radio emission in pulsars, this defines regimes where photon splitting might seed *radio quiescence* in SGRs and AXPs. Clearly there are some recently-discovered pulsars above the boundary, a situation contrasting the complete demarcation highlighted in [55] that pertained to the Princeton Catalogue era.

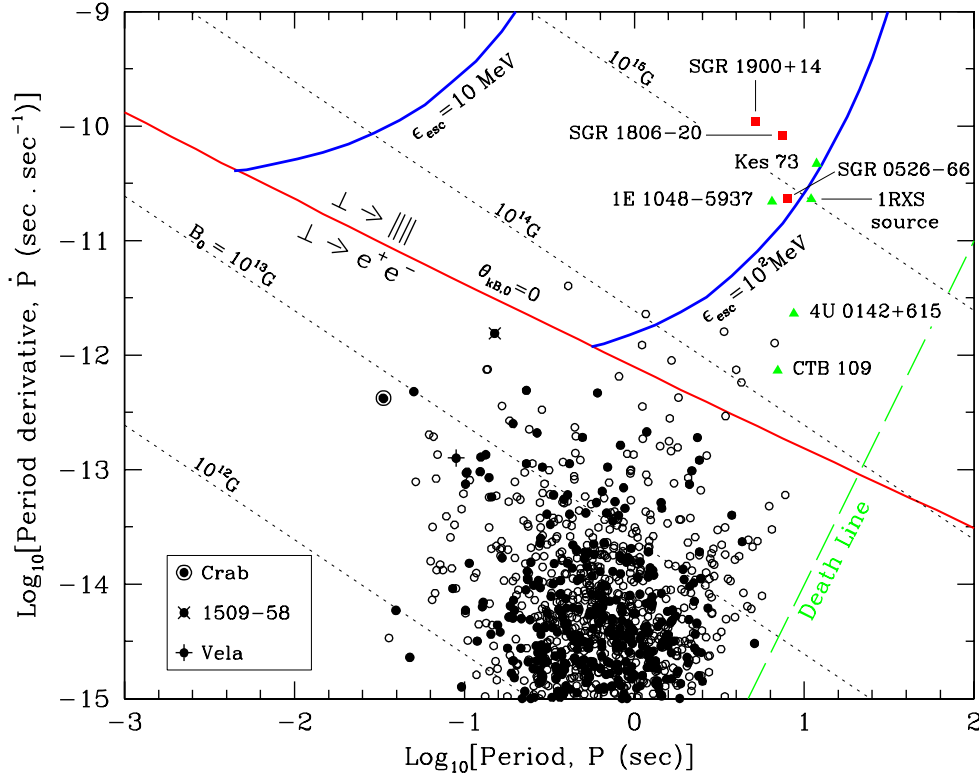


Fig. 3: The upper portion of the P - \dot{P} diagram, with filled circles denoting the locations of 541 members of the Princeton Pulsar Catalogue [56], and open circles marking 1599 radio pulsars in the more recent ATNF Pulsar Catalogue [57] (only those with $\dot{P} \geq 10^{-15}$ are visible). The approximate boundary (diagonal red line) demarcating when splitting dominates (uppermost \dot{P}) and when pair creation is prolific (lower \dot{P} for conventional pulsars) is indicated, being computed in [17]. Above this, the heavy-weight curves labelled $\varepsilon_{\text{esc}} = 10 \text{ MeV}$ and $\varepsilon_{\text{esc}} = 10^2 \text{ MeV}$ are contours for the escape energy of photon splitting, $\perp \rightarrow ||||$; to the right of these, the magnetosphere is transparent to 10 MeV and 100 MeV photons, respectively.

The placement of the quiescence boundary in the Figure presumes that the emission region is very near the stellar surface, a criterion that was specifically adopted when identifying the boundaries in Figure 3. If the altitude R_0 of the photon attenuation locale moves above the surface, then the putative radio quiescence boundary correspondingly moves to higher \dot{P} , i.e. higher surface polar fields B_0 . Since the local dipole field scales as $B \sim B_0(R_0/R_{\text{NS}})^{-3}$, which is pinned by the balanced competition between pair creation and splitting, and the inferred value of B_0 scales with observables as $B_0 \propto (\dot{P}P)^{1/2}$, the location of the quiescence boundary in the P - \dot{P} diagram approximately obeys $\dot{P} \propto R_0^{+6}$ for fixed pulsar periods P (and therefore also fixed polar cap angular sizes). Hence, small increases in R_0 above R_{NS} can easily [17] move the boundary above the radio pulsar population displayed in the

Figure. It should be emphasized that if Adler's splitting selection rules [24] apply here, then photons of \parallel polarization are only subject to pair creation. This implies only a partial suppression of $\gamma \rightarrow e^+e^-$ by splitting, which may lead to a postponement of pair creation eventually to higher altitudes [17]. However, photons of \perp polarization dominate the photon population generated by the principal primary and secondary emission processes of polar cap models for γ -ray pulsars [12, 38], namely cyclotron/synchrotron radiation, curvature emission and resonant Compton scattering. Hence, the partial suppression of pair creation by photon splittings $\perp \rightarrow \parallel$ is in fact likely to be quite effective at typical magnetar field strengths.

While this identifies a signature and observable action of photon splitting in an astrophysical setting, the connection to radio emission is the weak link in this logical construct. The commonly-held belief that the presence of a profusion of pairs is requisite for strong radio emission is not yet proven. The actual nature of the coherent radio emission process(es) is still unknown, a major problem in the study of pulsars. If the density of pairs is not relevant for the production of bright radio emission, then the action of splitting in magnetar field regimes has no formal connection to the observed radio quiescence or faintness of SGRs and AXPs. Hence this property cannot, at present, be regarded as a definitive measure of the action of splitting in pulsars. For potentially more direct evidence for the operation of $\gamma \rightarrow \gamma\gamma$ in pulsars, one turns again to spectroscopic evidence similar to that discussed in Section 4.1 for pair creation. Noting the maximum energy contours in Figure 3, for magnetars and pulsars with fields above 4×10^{13} Gauss, photon splitting should prohibit any emission above ~ 100 MeV, though prominent signals below 100 MeV are possible [58] due to the efficiency of resonant Compton upscattering of surface thermal X-ray photons. Accordingly, photon splitting should generate the spectral turnovers in supercritical fields, not solely pair creation, and the physics of the process guarantees that the cutoff energies are polarization-dependent. This effect was discussed in [41], where a focal study of the high-field pulsar PSR 1509-58 indicated that the observed spectral data in the sub-100 MeV range implied a cutoff that could only be modelled in a polar cap scenario if photon splitting was acting in addition to general relativistic effects. The data for this pulsar do not permit much play in the parameter space, so the inference that splitting is active in PSR 1509-58 is quite strong. Yet it is crucial to find one or more other high- B pulsars where such constrained inferences can be made. Unfortunately such a prospect is not yet on the horizon. While NASA's imminent GLAST mission will discover an array of new gamma-ray pulsars, this issue can only be addressed by a sensitive, next-generation telescope in the 1–30 MeV range such as the Advanced Compton Telescope. Yet this specific science question, acquiring strong evidence for the action of an untested prediction of strong-field QED, forms part of the many motivations for developing a new medium-energy gamma-ray mission that has polarimetric capability.

5 Conclusion

Two of the exotic and fascinating predictions of quantum electrodynamics in strong magnetic fields have been highlighted in this paper, one-photon pair creation and photon splitting. It is an impressive indicator of the confidence placed in the theory of QED by physicists that, in spite of a lack of experimental vindication in terrestrial laboratories, they are both calculated theoretically in spite of significant degrees of mathematical complexity (particularly for photon splitting), and anticipated almost routinely in the astrophysical context of pulsars and elsewhere. There have been various limited attempts to explore these processes in laboratories, sometimes indirectly by searching for birefringence signatures using lasers in optical cavities [59, 60], but so far without definitive results. Largely this is because the required fields are beyond present experimental capabilities: for $B \sim 1$ MGauss, super-TeV energy photons are required to start to approach the criterion $\omega B \gtrsim 0.1$ (in dimensionless units) for $\gamma \rightarrow e^+e^-$ to become significant. It is not beyond reason that building from the status quo of current powerful terrestrial magnets and particle accelerator technology such as the Large Hadron Collider (LHC), it may prove possible to access the appropriate ω - B phase space in a laboratory setting in the coming decades. In the meantime, it is of great interest to explore their application to astrophysics, not just to anticipate an alternative proof of the action of these QED processes, but also to enhance our understanding of the exotic cosmic sources, specifically pulsars, that can provide a conducive environment for the activity of $\gamma \rightarrow e^+e^-$ and $\gamma \rightarrow \gamma\gamma$.

Acknowledgements I thank Dr. Alice Harding and Prof. Don Melrose for many collaborative insights over the years relating to QED processes in strong magnetic fields, and Dr. Ken Hines (deceased) for starting me on my way in this field.

References

- [1] Hoyle, F., Narlikar, J. V. & Wheeler, J. A. (1964), *Nature*, 203, 914.
- [2] Shapiro, S. T. & Teukolsky, S. A. (1983), *Black Holes, White Dwarfs and Neutron Stars: The Physics of Compact Objects* (Wiley & Sons, New York).
- [3] Hewish, A., Bell, S. J., Pilkington, J. D. H., et al. (1968), *Nature*, 217, 709.
- [4] Gold, T. (1968), *Nature*, 218, 731.
- [5] Sturrock, P. A. (1971), *ApJ*, 164, 529.
- [6] Ruderman, M. A. & Sutherland, P. G. (1975), *ApJ*, 196, 51.
- [7] Trümper, J., Pietsch, C., Reppin, W., et al. (1978), *ApJ Lett.*, 219, L105.
- [8] Daugherty, J. K. & Harding, A. K. (1986), *ApJ*, 309, 362.
- [9] Bussard, R. W., Alexander, S. B. & Mészáros, P. (1986), *Phys. Rev. D*, 34, 440.

- [10] Sokolov, A. A. & Ternov, I. M. 1968, *Synchrotron Radiation* (Pergamon Press, Oxford).
- [11] Baring, M. G. (1988), MNRAS, 235, 79.
- [12] Daugherty, J. K. & Harding A. K. (1982), ApJ, 252, 337.
- [13] Toll, J. S. (1952), Ph.D. Thesis, Princeton University.
- [14] Klepikov, N. V. (1954), Zh. Eksp. Theor. Fiz., 26, 19.
- [15] Daugherty, J. K. & Harding A. K. (1983), ApJ, 273, 761.
- [16] Baier, V. N. & Katkov, V. M. (2007), Phys. Rev. D, 75, 073009.
- [17] Baring, M. G. & Harding A. K. (2001), ApJ, 547, 929.
- [18] Erber, T. (1966), Rev. Mod. Phys., 38, 626.
- [19] Tsai, W.-Y. & Erber, T. (1974), Phys. Rev. D, 10, 492.
- [20] Shabad, A. E. & Usov, V. V. (1985), Astr. Space Sci., 117, 309.
- [21] Herold, H., Ruder, H. & Wunner, G. (1985), Phys. Rev. Letters, 54, 1452.
- [22] Usov, V. V. & Melrose, D. B. (1995), Aust. J. Phys., 48, 571.
- [23] Baring, M. G. & Harding A. K. (1997), ApJ, 482, 372.
- [24] Adler, S. L. (1971), Ann. Phys., 67, 599.
- [25] Mitrofanov, I. G., Pozanenko, A. S., Dolidze, V. Sh., et al. (1986), Sov. Astron., 30, 659.
- [26] Jauch, M. M., & Rohrlich, F. (1980), *The Theory of Photons and Electrons* (2nd edn. Springer, Berlin).
- [27] Bialynicka-Birula, Z., & Bialynicki-Birula, I. (1970), Phys. Rev. D, 2, 2341.
- [28] Adler, S. L., Bahcall, J. N., Callan, C. G., & Rosenbluth, M. N. (1970), Phys. Rev. Letters, 25, 1061.
- [29] Stoneham, R. J. (1979), J. Phys. A, 12, 2187.
- [30] Baier, V. N., Mil'shtein, A. I., & Shaisultanov, R. Zh. (1996), Phys. Rev. Letters, 77, 1691.
- [31] Adler, S. L. & Schubert, C. (1996), Phys. Rev. Letters, 77, 1695.
- [32] Mentzel, M., Berg, D., & Wunner, G. (1994), Phys. Rev. D, 50, 1125.
- [33] Weise, J. I., Baring, M. G. & Melrose, D. B. (1998), Phys. Rev. D, 57, 5526.
- [34] Baring, M. G. (2000), Phys. Rev. D, 62, 016003.
- [35] Shabad, A. E. (1975), Ann. Phys., 90, 166.
- [36] Bulik, T. (1998), Acta Astron. 48, 695.
- [37] Weise, J. I. & Melrose, D. B. (2006), Phys. Rev. D, 73, 045005.
- [38] Daugherty, J. K. & Harding A. K. (1996), ApJ, 458, 278.

- [39] Thompson, D. J. (2001), in *High Energy Gamma-Ray Astronomy*, eds. F. A. Aharonian, H. Völk, AIP Conf. Proc. 558, 103.
- [40] Baring, M. G. (2004), *Adv. Space Res.*, 33, 552.
- [41] Harding A. K., Baring, M. G. & Gonthier, P. L. (1997), *ApJ*, 476, 246.
- [42] Bulik, T. B. Rudak, B. & J. Dyks (2000), *MNRAS*, 317, 97.
- [43] Harding A. K., Usov, V. V. & Muslimov, A. G. (2005), *ApJ*, 622, 531.
- [44] Razzano, M. & Harding, A. K. (2007), in *The First GLAST Symposium*, eds. S. Ritz, P. F. Michelson & C. Meegan (AIP Conf. Proc. 921) p. 413.
- [45] Lei, F., A. G. Dean & G. L. Hills (1997), *Space Sci. Rev.* 82, 309.
- [46] Coburn, W. & Boggs, S. E. (2003), *Nature* 423, 415.
- [47] Kalemci, E., Boggs, S. E., Kouveliotou, C., Finger, M. & Baring, M. G. (2007), *Astrophys. J. Supp.*, 169, 75.
- [48] Boggs, S. E. (2006), *New Astr. Rev.*, 50, 604. [for the Advanced Compton Telescope, see also: <http://www.ssl.berkeley.edu/act/>]
- [49] Risse, M., Homola, P., Góra, D., et al. (2004), *Astroparticle Phys.*, 21, 479.
- [50] Risse, M., Homola, P., Engel, R., et al. (2005), *Phys. Rev. Letters*, 95, 171102.
- [51] Vasisht, G. & Gotthelf, E. V. (1997), *ApJ*, 486, L129.
- [52] Hurley, K. et al. 1999, *Nature*, 397, 41.
- [53] Shitov, Yu. P., Pugachev, V. D. & Kutuzov, S. M. (2000), in *Pulsar Astronomy: 2000 and Beyond* eds. M. Kramer, et al., (ASP Conf. Ser., San Francisco), p. 685.
- [54] Camilo, F., Ransom, S. M., Halpern, J. P., et al. (2006), *Nature*, 442, 892.
- [55] Baring, M. G. & Harding A. K. (1998), *ApJ*, 507, L55.
- [56] Taylor, J. H., Manchester, R. N. & Lyne, A. G. (1993), *ApJ Supp.*, 88, 529.
- [57] Manchester, R. N., Hobbs, G. B., Teoh, A. & Hobbs, M. (2005) *Astron. J.*, 129, 1993. [see also the ATNF Pulsar Catalog database at <http://www.atnf.csiro.au/research/pulsar/psrcat/>]
- [58] Baring, M. G. & Harding A. K. (2007), *Astrophys. Space Sci.*, 308, 109.
- [59] Cameron, R., Cantatore, G., Melissinos, A. C., et al., (1993), *Phys. Rev. D*, 47, 3707.
- [60] Zavattini, E., Zavattini, G., Ruoso, G., et al., [PVLAS Collaboration] (2007), *Phys. Rev. Letters*, 99, 129901. [See preprint [hep-ex/0706.3419](#) for details].